Penetration of Ar and He RF-driven plasma jets into micrometer sized capillary tubes.

A Thesis
SUBMITTED TO THE FACULTY OF
UNIVERSITY OF MINNESOTA
BY

Amita Brahme

IN PARTIAL FULFILLMENT OF THE REQUIREMENTS
FOR THE DEGREE OF
MASTER OF SCIENCE

Adviser: Dr. Peter J. Bruggeman

July 2018

Acknowledgements

Firstly, I would like to thank my adviser, Dr. Peter J. Bruggeman for his endless support and accurate guidance for my Master's research. I am forever grateful for his patience and help in making me understand the concepts. Master's work would not have been possible without his immense knowledge and critical analysis. Completing the thesis from out of the state was only possible because of his availability over phone and email whenever I needed. It is not just the research but his insights in choosing my Master's coursework were also important and helpful. I am truly thankful for the advisory role he played during my Master's degree.

This work has been supported by the Department of Energy and I thank them for the support.

I would like to thank my research colleagues Zhengshi Chang and Ni Zhao for their contribution in experimentation and thesis writing. I appreciate their help in solving formatting issues of my thesis.

I would like to thank PhD student, Santosh Kondeti, who taught me the operation and power measurement of RF jet. I learnt operations of instruments like ICCD Camera from him. I appreciate his eagerness and will to help whenever I asked for. I would also like to thank PhD student Gaurav Nayak for his support and encouragement during my Master's research. He helped in learning COMSOL-Multiphysics which was an essential requirement for analysis. I thank them and my other fellow lab mates, Yuchen Luo and Eveline van Doremaele for the stimulating discussion and help.

My special thanks go to the DGS, ME dept., Dr. Chris Hogan for his support in figuring out a way to complete master's plan A while simultaneously working as a co-op in Lennox International, Dallas, Texas.

I would like to thank my manager, Umesh Gokhale and director of Applied Research department, Ajay Iyenger at Lennox International for constant encouragement for thesis plan during my Master's.

Last but not the least, I would like to thank my family, my parents and my sister. I would not be here at this milestone today if it wasn't for them. Thanking them is disrespecting their unconditional love for me. I cannot imagine surviving in another country without the feeling that they are always there for support and decision making, no matter what. I am also thankful to my dearest friends Mangesh, Shalaka and Chinmay for making me believe in myself and encouraging me whenever I felt low.

Amita Brahme

Dedication

This thesis is dedicated to my Parents, Mrs. Harsha Brahme and Mr. Anand Brahme, for their love, constant support and encouragement.

Abstract

The penetration and propagation of cold atmospheric pressure plasmas into volumes having sub-millimeter to micrometer sizes with large aspect ratios is required for enabling an effective disinfection of the inside of catheter tubes, tooth cavities, skin pores and enhance plasma catalysis in porous catalysts. As filamentary plasmas have often a characteristic diameter on the same length scale as tubes or pores, the penetration of plasma in these tubes and pores is not a priori obvious and can have a huge effect on the plasma properties. Particularly for medical applications, especially on teeth and skin, it is important that the plasma operates at low voltages and near ambient gas temperatures. This study has a goal to complement existing research in this area that has mainly been focused on pulsed discharges with significant over-voltage.

We report on a study using RF driven argon and helium plasma jets with the plasma generation outside the capillary followed by its penetration and propagation inside the capillary. We present the experimental determination of the limitations on the penetration diameter, and the underpinning mechanisms of the plasma propagation and penetration process. Experimental results include time resolved imaging of plasma propagation and penetration in capillaries with different internal diameter and report surface electric field measurements.

We found that the time between the plasma jet in first contact with the capillary tube surface and the subsequent penetration into the capillary tube spans several RF cycles due to electric fields at the plasma-tube interface below 4 kV/cm. These low electric fields require Penning ionization and/or stepwise ionization and hence a build up of the metastable and electron density to achieve a locally sufficiently large ionization rate to enable penetration and propagation. Furthermore, it is found that the propagation of the argon jet into the capillary occurs during the positive half cycle of the RF waveform and is very similar to the propagation of the jet in surrounding air.

Table of Content

List of Tables

List of Figures

Introduction

Low temperature plasmas have been intensively studied for the last two decades in the context of many applications including environmental remediation, disinfection and medical applications [1-4]. These applications have been enabled by the development of plasma sources operating near ambient temperatures enabling the treatment and disinfection of heat sensitive surfaces including polymers, unprocessed food and living tissue without thermal damage [5,6,7]**.**

Plasma treatment has also been proposed for the decontamination of devices such as catheters and endoscopes and even tooth cavities. In this case, plasma penetration and propagation into volumes having sub-millimeter to micrometer sizes with large aspect ratios such as capillary tubes, is required for enabling an effective treatment and advance the applications in this area. Nonetheless, the underpinning mechanisms of plasma penetration and propagation in micrometer-sized capillaries are currently not fully understood.

The penetration of plasmas in micro and nano-sized pores is also of importance in plasma catalysis. Plasmas have been shown to enhance chemical conversions in catalytic processes in the context of environmental remediation and energy applications. This includes gaseous pollutants removal, hydrocarbon reforming, and the conversion of greenhouse gases into value added chemicals. Many catalysts are porous and the interaction of the plasma with the active component of the catalytic material in the pores is crucial for enhancing the plasma-catalytic synergistic enhancement of the conversion process [8,9]. It is reported that enhanced surface electric fields can assist micro-discharge formation inside pores and aids in the generation of short-lived charged and reactive species believed to be responsible for the reported synergistic effect between plasma and catalysts [8].

Previous research of the penetration and propagation of plasma into pores with a large aspect ratio has been studied through fluid model simulations of an atmospheric pressure dielectric barrier discharge (DBD) in helium to analyze the characteristics of plasma inside the micro-pores of porous catalysts [9]. Bogaerts *et al* [8,9] report a minimum diameter of 200 μm below which helium DBD plasma does not penetrate inside the pore. This result is however dependent on the applied voltage [8,9]. While research has been reported in the area of plasma generation inside capillary tubes in helium with different diameter [14-16, 24], an experimental study on the penetration of helium plasmas in micro-cavities or capillaries is to our knowledge not reported. The generation of discharges in an array of capillaries has been reported to enable the generation of large volume atmospheric pressure plasmas [10]. Nonetheless, the focus of these studies was on the large volume plasma and not the generation of the plasma inside the capillary.

An experimental study of AC driven helium discharges in capillary tubes reported that the minimum required voltage to sustain a discharge in a capillary, increases with decreasing diameter [23]. This increase in voltage with decreasing diameter is required to increase the ionization rate to compensate for the enhanced loss of electrons to the capillary wall due to a decreasing diffusion length with decreasing diameter [23]. The minimum pore size in ceramic capillaries in which air or N_2 streamer plasma discharge can sustain is of the order of 2-10 μm, considerable less than for the above mentioned minimum diameter for a diffuse helium discharge [11]. This difference is attributed due to a significant difference in electron density between a filamentary discharge in air and a diffuse glow discharge in helium. The larger Debye length for the helium discharge, which is of the order of tens to hundred micrometers does not allow the penetration of the sheath into the capillary [12].

Most of the research carried out so far has been focused on conditions with high amplitude applied voltages, not always suitable for applications such as medical treatments on skin or in teeth cavities. The underlying paper complements previous studies by reporting a study using RF driven argon and helium plasma jets which has the plasma generation outside the capillary followed by its penetration and propagation inside the capillary. While discharges generated by pulsed voltages often are generated with significant over-voltages (i.e. the applied voltage is larger than the DC breakdown voltage) RF driven plasmas are generated by relative low voltages and operate near the breakdown threshold. In addition, the RF driven plasma jet can be used for heat sensitive treatments at low operating powers [13].

The objectives of our study include the experimental determination of the limitations on the penetration diameter, and the determination of the underpinning mechanisms of the plasma propagation and penetration process. We present time resolved imaging of plasma propagation and penetration in capillaries with different internal diameter and report surface electric field measurements. These measurements are complemented with an analysis of the ionization and electron recombination processes to explain the observations.

2. Experimental Setup and Methods

2.1 Plasma setup and electrical characterization

Figure 1 shows a schematic of the experimental setup and plasma source used in this work. The plasma source is an atmospheric pressure RF-driven plasma jet identical to the plasma jet used in [13,19]. The plasma jet consists of a quartz tube with an inner diameter of 2 mm containing an RF-driven tungsten needle electrode with a diameter of 1 mm. A grounded ring electrode with a height of 5.25 mm, is placed around the outside of the quartz tube 0.9 mm above the nozzle. All reported experiments were performed with argon or helium flowing through the tube at 1.5 standard liter per minutes (slm). The plasma jet was operated in ambient air. The temperature and relative humidity of the ambient air in the laboratory were stable and equal to 21-22°C and 30 %.

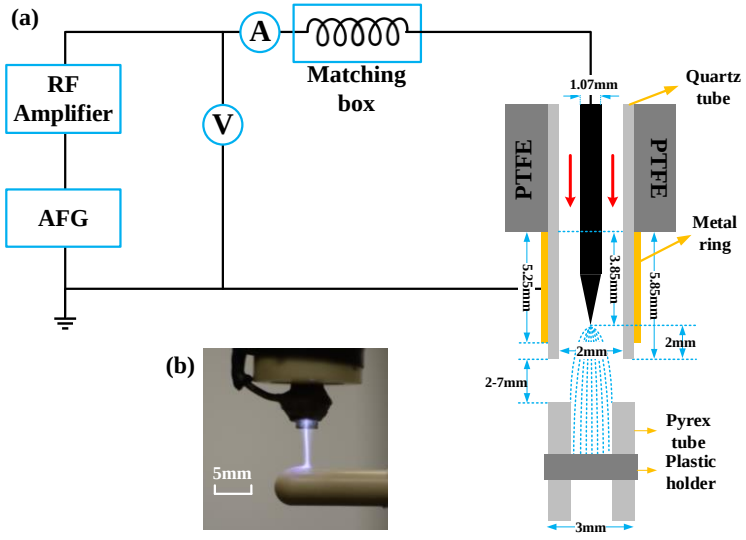

Figure 1: (a) Schematic of the plasma jet during the interaction with capillary tube (b) Image of the plasma jet impinging on the electric field probe. AFG: arbitrary function generator.

The plasma was generated by applying an RF high voltage sinusoidal waveform to the needle electrode with a frequency of 13.3 MHz modulated at a

frequency of 20 kHz with a 20% duty cycle. The plasma was thus on for 10 μs and off for 40 μs. This RF waveform was generated by an arbitrary function generator (Tektronix AFG 2021) and amplified by an RF amplifier (Amplifier Research 75A250A). The output of the amplifier was connected through a homemade matching box consisting of an inductance to match the impedance of the plasma with the power supply. Current and voltage waveforms were recorded by an oscilloscope (Tektronix DPO 2024 B) by connecting a Rogowski coil (Pearson 2877) and a voltage probe (Tektronix P5100A) at the locations as indicated in figure 1. The plasma-dissipated power was calculated from these measurements as described in detail in [22]. The time averaged plasma dissipated power was kept constant at 2.5W throughout this work. In view of the 20% duty cycle, the instantaneous plasma on power is equal to 10 W.

To investigate the penetration and propagation of the plasma in capillary tubes with an internal diameter between 100 μm and 1.5 mm, Pyrex glass capillary tubes with a fixed outer diameter of 3 mm outer diameter were positioned under the nozzle of the plasma jet. The tolerance on the inner diameter of the tubes, as reported by the manufacture, is 5%. The tube was held in a tube holder and mounted on an x-y-z translation stage allowing us to adjust the position of the capillary with the plasma jet through micrometer screws with an accuracy of 10 μm. The distance between the plasma jet nozzle and the upper end of the capillary was varied between 2 and 7 mm.

2.2 Imaging

Color images of the plasma jet interacting with capillaries with different internal diameter were taken by a CCD camera (Nikon D3100). An intensified charged coupled device (ICCD Andor iStar DH340T-25U-03) with a lens (zoom 7000 Navitar TV zoom Japan) was used to perform time resolved imaging of the plasma

propagation in and outside the capillary tube and the penetration process. The ICCD camera was triggered by the RF modulation signal produced by the signal generator. Images were taken with different delays to capture the entire plasma-on cycle with a gate of 50 ns. Each image consists of 50 accumulations.

The RF signal was drifting slowly compared to the modulation signal and this approach does not allow detailed phase resolved measurements. The phase resolved measurements presented in this work were obtained by using a different signal generator (AFG3051C) enabling a fixed phase difference between RF signal and modulation signal at an RF frequency of 12.16 MHz. All other parameters were kept identical. The gate of the camera in this case was equal to $1/4^{th}$ of the period of the discharge.

2.3 Electric Field Measurement

To estimate the electric field at the position where the plasma touches the upper part of the capillary tube, we used an electro-optic sensor developed by Kapteos S.A.S. As the electric permittivity of Pyrex glass (4.6) [34] and outer insulation of Kapteos probe (3.3) is comparable, a measurement of the plasma in contact with the sensor was used as a representative estimate of the electric field of the plasma in contact with the capillary. This sensor (P1tR05-BS1-air) connected to an amplifier and laser unit (eoSense MF-01U-2-AMP) that has a 50 Ω signal output id read out by an oscilloscope (Tektronix DPO 2024B) allowing time synchronized measurements with the voltage and current waveforms. This sensor, based on the Pockels effect, allows measuring electric fields with a time resolution down to 1 ns. The sensor is made of a cylindrical isotropic birefringent crystal probed with a laser beam guided through the crystal. Depending on the variation of the light polarization induced by

the external electric field in the crystal, the system can measure the transverse electric field. While the crystal, with a diameter of 1 mm, allows measuring the electric field with a resolution of 1 mm, the crystal is inside a cylindrically shaped dielectric with a diameter of 5 mm. This outer insulation significantly reduces the spatial resolution of the measurement.

The electric field probe was calibrated in a homogenous electric field providing a so-called antenna factor (AF) converting the measured voltage amplitude in an averaged electric field amplitude inside the crystal. However, we require the electric field at the outside dielectric surface of the probe in contact with the plasma. A model is required to deduce the surface electric field from the measured electric field in the crystal. The calibration and the calculation procedure to obtain the surface electric field are reported in detail in the next section.

2.4 Electric Field Calibration

We performed a calibration of the electric field probe in a homogeneous electric field in a parallel plate capacitor as shown in figure 2(a). Instead of calibrating the probe with the applied electric field, we calculate the electric field distribution and correlate the output voltage of the electro-optic sensor with the simulated electric field inside the crystal. This allowed us to determine an antenna factor that converts the measured voltage amplitude in the electric field amplitude inside the crystal. The exact geometry of the probe and the dimensions of the capacitor used to apply a homogeneous electric field to the probe is shown in the figure 2(a). In the homogeneous field condition, the probe is modeled in air between two circular plates, one of which is subjected to a high voltage and the other is a grounded electrode. The

normal derivate of the voltage is set zero at the radial boundary of the computational domain.

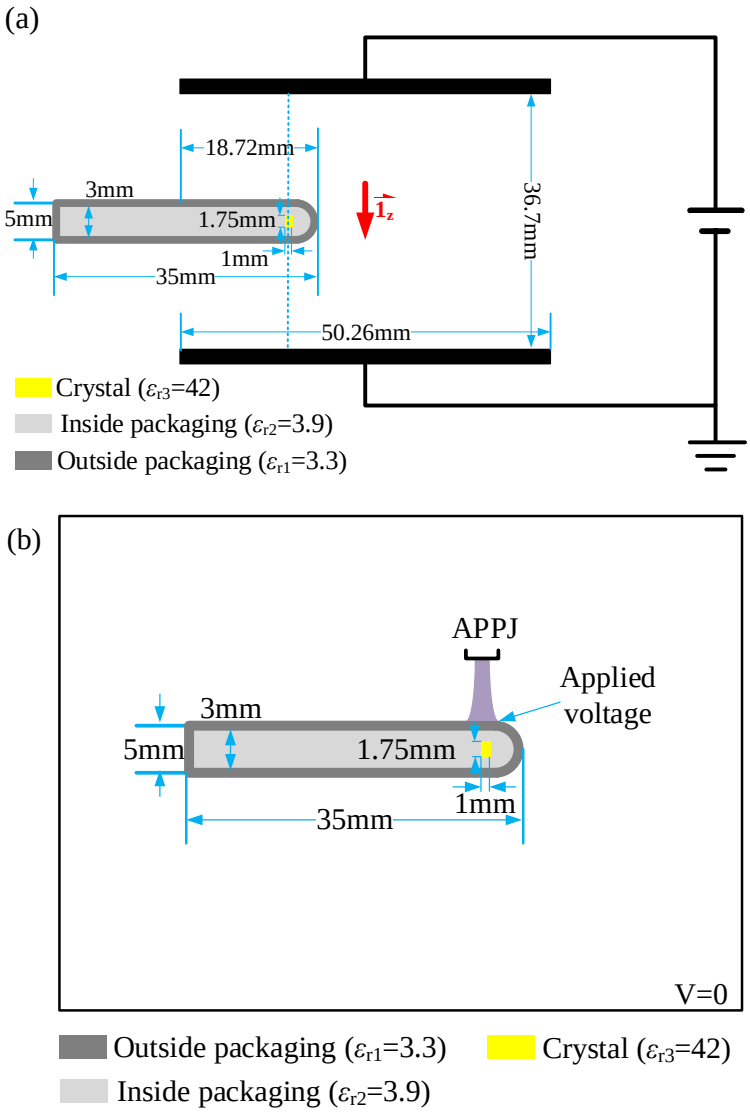

Figure 2: (a) Schematic of the configuration used to calibrate electric field inside the probe crystal. (b) Schematic of the computational domain and approach used to calculate the plasma-probe interfacial electric field.

Figure 3 shows the electric field component E_z along the dashed line shown in figure 2 (a). The electric field distribution at the probe interface and inside the probe is highly inhomogeneous due to the large changes in dielectric constants of the different probe materials. Measuring the induced voltages by the electric field probe

for different applied homogeneous electric fields allowed us to construct the calibration curve shown in figure 4. For the current system, the antenna factor determined from this graph is equal to $5.34 \pm 0.03 \times 10^5$ m^{-1}. The measurements are performed in the linear part of the calibration curve.

To convert the measured electric field in the crystal to the electric field amplitude at the plasma-probe interface we simulated this situation by considering the plasma as a given uniform voltage boundary condition. The area of the applied voltage was chosen to be equal to area of the visible plasma emission zone at the interface and twice that value. This approach is motivated by earlier work performed by Wild and Stollenwerk [25] suggesting that the charge distribution can be twice as large as the visual emission. The reported electric field is an average of these two conditions and the corresponding standard deviation of these two values with the variation in the experimentally recorded AF factor (e.g. due to temperature changes of the crystal) constitutes the reported uncertainty.

To obtain the correlation of the measured electric field inside the crystal with the electrical field at the plasma-probe interface, we varied the applied voltage in the simulation until the simulated electric field inside the crystal corresponded to the measured electric field. The electric field at the interface can then be determined from the simulation. Figure 2(b) shows the computational domain of the non-homogeneous field calculation. The probe is enclosed in a grounded cuboid at a minimum distance from the probe equal to 5 probe diameters to ensure the boundary does not have a significant impact on the calculated electric field inside the probe. All 3-dimensional simulations were performed with COMSOL Multiphysics.

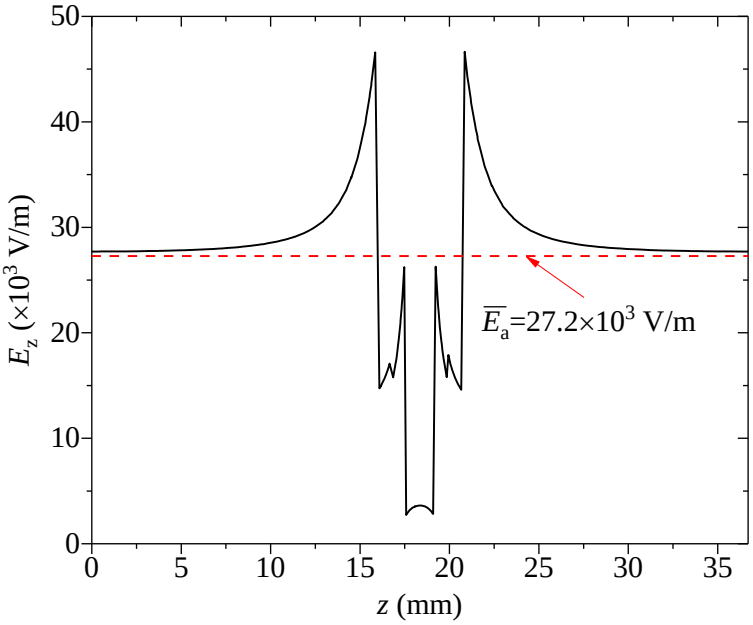

Figure 3: **Electric field in z- direction (E_z) as a function of position along the blue dotted line in Figure 2 (a).**

The 3-dimensional simulations were performed in COMSOL Multiphysics AC/DC Module. Figure 2 (b) shows the computational domain of the non-homogeneous field calculation. The probe is enclosed in a grounded cuboid at a minimum distance from the probe equal to 5 probe diameters to ensure the boundary does not have a significant impact on the calculated electric field inside the probe.

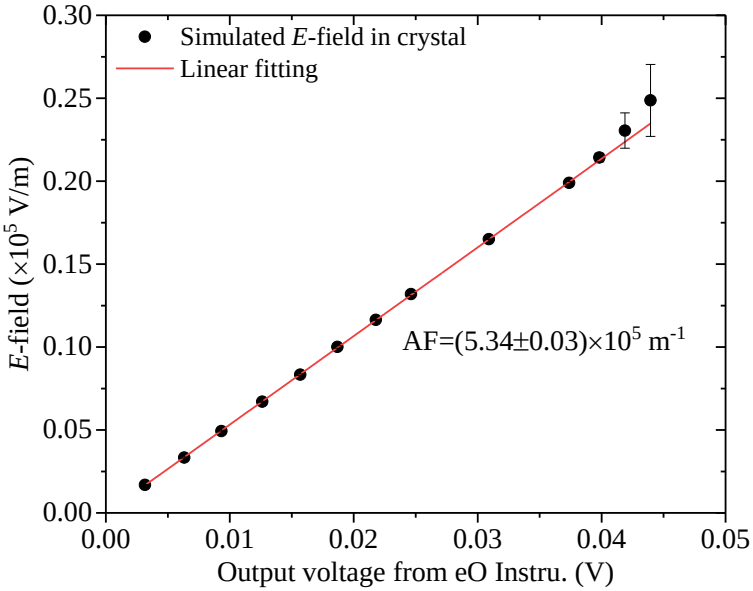

Figure 4: Electric field inside crystal in z- direction (E_z) as a function of measured output voltage. The z_p direction is defined in figure 2(a).

3. Results and Discussion

3.1 Plasma conditions

Figure 5 shows the voltage waveform and the period averaged on off and plasma dissipated power waveform for the argon plasma jet impinging onto a capillary with a 500 µm internal diameter at 4 mm. The voltage and power are independent of the presence of a capillary tube. Similar waveforms are also obtained for the helium plasma jet.

Comparing the plasma on and off power waveform shows that the initial peak in power is due to the charging of the equivalent capacity of the plasma jet. A steady state power is achieved 1 µs after the RF voltage is switched on. This result is consistent with reported time resolved emission spectra and electron density measurements that indeed shows several RF cycles are required to achieve a steady state electron density and strong emission at a fixed position [17,19]. This steady state power is achieved well before the plasma plume touches the capillary at 2.2 µs.

The measured electric field corresponding to the electric field inside the crystal is also shown in figure 5. The electric field waveform strongly correlates with the propagation of the plasma filament and exhibits a significant growth until the plasma is in contact with the probe. Indeed, the induced electric field by the conductive plasma plume connected to the RF driven needle electrode is significantly larger than the Laplacian electric field generated by the needle electrode without plasma formation. Mass spectrometry measurements in the effluent of the same jet showed that the ion flux drops only by a factor of 10 over 4 mm [21]. Hence, a significant flux of electrons and ions towards the substrate is also expected when the plasma is not in direct contact with the dielectric probe surface. In addition, the electric field waveform is asymmetric with a negative bias due to the (on average)

negative surface charge caused by the electron flux toward the dielectric surface when the plasma is in contact with the dielectric surface.

While the amplitude of the electric field depends on the gas (He or Ar) and the distance between the jet nozzle and the capillary as it correlates with the plasma plume length, the electric field waveforms remain similar for the different conditions investigated in this work. Nonetheless the measured electric field amplitude for helium is smaller than for argon at the same distance (see also further).

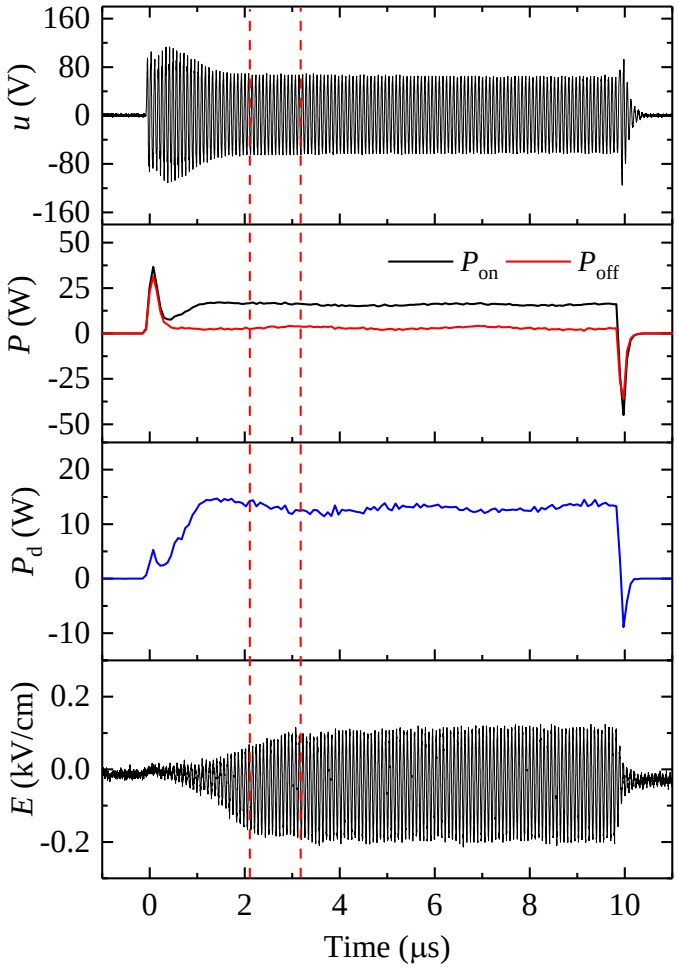

Figure 5: Plot of RF voltage, period averaged plasma on (P_{on}), plasma off (P_{off}) and plasma dissipated (P_d) power and measured electric field at the position of the crystal with respect to time for the argon plasma jet impinging on a 500 µm capillary tube at distance of 4 mm from the nozzle. The red dashed lines indicate the time at which the plasma jet is in contact with the capillary tube edge and penetrates the capillary tube respectively. The positive direction of the electric field is the same as the direction of the gas flow from the jet.

Table 1 provides an overview of the typical plasma properties of the studied plasma jet. The gas temperature for both argon and helium can reach 450 K at the nozzle, however, the gas temperature drops quickly below 350 K at a distance of 5 mm from the nozzle [19]. The electron temperature in such plasmas is typically of the order of 2 eV. This has been confirmed by Thomson scattering measurements in a similar RF jet in argon yielding electron temperatures between 1 and 2 eV [17]. Electron densities in argon as measured by Thomson scattering are between 10^{19} and 10^{20} m-3 [17]. The electron density in similar helium plasma jets has been estimated based on power density and is in the range of $10^{17} – 10^{18}$ m^{-3} [20]. With these typical values we can estimate the Debye length for both gases. The Debye length for argon is one order of magnitude less than the Debye length of helium and both are smaller than the minimum capillary diameter of 100 µm for which no penetration is observed. Nonetheless, the Debye length of the helium jet has a similar value as the capillary diameter and might be a limiting factor in the formation of two for the penetration of a sheath into the capillary tube and the formation of a sheath at the plasma-capillary wall interface when the ionization front propagates into the capillary tube.

	Argon jet	Helium jet
T_{gas} (K)	300-350	300-350
T_e (eV)	2	2
n_e (m^{-3})	10^{19} - 10^{20}	5×10^{17} - 5×10^{18}
λ_d (µm)	0.1 - 3	20 – 66

Table 1: Typical gas temperatures, electron densities and temperatures for the argon and helium plasma jet effluent investigated in this work [17, 19, 20]. The Debye length calculated based on these parameters is also provided.

.

3.2 Penetration conditions

We studied the interaction of the helium and argon plasma jet with capillary with internal diameters of 100, 150, 250, 500 μm and 1.5 mm inner diameter at a distance of 4 mm between the nozzle and the capillary tube surface. Figure 3 shows representative images of the argon and helium plasma jet interacting with the capillary with an internal diameter of 250 and 500 μm. Both argon and helium, plasma penetrates in a 500 μm capillary tube. However, in the case of argon the plasma is able to propagate a few centimeters into the capillary, while the helium jet penetrates the 500 μm capillary, no significant propagation of the helium plasma plume into the capillary tube is observed in excess of 1.2 mm. Both the argon and the helium jet do not penetrate into a 250 μm capillary tube. However, an additional different behavior for helium and argon is found when a grounded metal ring electrode was placed around the tube at 2 cm from the capillary tube edge. In this case the argon plasma jet penetrates and propagates into the 250 μm capillary tube most likely due to the local enhancement of the electric field by the grounded ring electrode. This suggest that the minimum penetration diameter is close to 250 μm for the argon plasma jet but is larger than 250 μm for the helium plasma jet. We confirmed that the argon plasma jet, in the presence of the metal electrode is not able to penetrate in a capillary with a diameter of 150 μm.

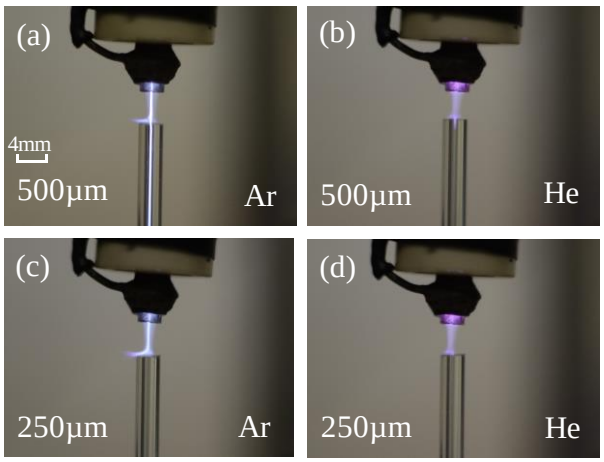

Figure 6: CCD images of the argon and helium plasma jet impinging onto capillary tubes at a distance of 4 mm. The capillary tube inner diameter and gas is noted in each image. Penetration is only found for the 500 µm capillary tube diameter for both argon and helium.

To understand the reason behind the observed differences in penetration ability between the helium and argon plasma jet, we compare the capillary diameters with the plasma plume diameter of the free jet for argon and helium which was found to be 340 ± 80 µm and 675 ± 80 µm respectively. The smallest capillary tube diameters in which penetration is observed are thus smaller than the diameter of the free jet.

When the plasma inside a capillary tube can has a smaller diameter than the actual diameter of the plasma in the free jet, the presence of the capillary will enhance the radial diffusion losses of charged species (and particularly electrons). This condition could influence the electron losses and alters the sustainment conditions of the plasma [23]. Table 2 shows the estimated radial losses of ions and electrons by diffusion and ambipolar diffusion for tube diameters of 250 and 500 µm. Ion diffusion constants (D_i) are found using the Einstein relation

$$D_i = \mu K_B T_g / e, \qquad (1)$$

where "μ" is the ion mobility reported in [22], "k_B" is the Boltzmann constant, "T_g" is the gas temperature and *"e"* is the elementary charge. The corresponding diffusion loss time constants are calculated by

$$\tau = \left(\frac{R}{2.4}\right)^2 \Big/ D \qquad (2)$$

with R the radius of the capillary tube. Ambipolar diffusion constants (D_{amb}) are calculated from ionic diffusion constants using $D_{amb} = D_i\,(1+T_e/T_g)$. Electron diffusion constants are taken from [32]. While electron diffusion can be important during the initial penetration process, the time constant for ambipolar diffusion will be a more realistic time scale for electron loss by diffusion once the plasma is established in the capillary tube. Table 2 also estimates of the dissociative electron-ion dissociative recombination time, the time constant of the dominant bulk electron loss mechanism, as calculated in [20]. Comparing the electron-ion dissociative recombination time with ambipolar diffusion clearly shows that bulk electron losses remain dominant for argon while for helium the ambipolar diffusion losses are similar to the bulk electron losses. Hence changes in diffusion losses will drastically impact the helium jet but not the argon jet. This is consistent with the limited penetration capability of helium even for the 500 µm capillary.

During the penetration process when the plasma is not fully formed in the capillary yet, an ambipolar field might not have been established yet in the capillary. The electron diffusion time constant is similar or larger than the RF period (~75 ns) for a 500 µm capillary tube while it drops significantly below the RF period for a 250 µm capillary tube. This suggests that electron loss cannot be sustained during one discharge period unless an ambipolar electric field is build up that reduces the

diffusion losses of the electrons. As the dissociative recombination time in argon is similar to the electron diffusion time even for the 250 μm capillary tube, the increased electron diffusion loss will be less significant in argon than in helium. This is consistent with the observations that the argon jet can penetrate in the capillary with an internal diameter of 250 μm in the presence of a grounded ring electrode and the helium plasma jet not. The argon plasma jet is unable to penetrate a capillary with an internal diameter of 150 μm even with a grounded ring electrode. In this case the electron diffusion time is 6.5 ns and becomes less than the dissociative recombination time.

The electron loss estimates correlate well with the ability of plasmas to penetrate capillaries and suggest that the formation of an ambipolar field in the capillary or an increased electron production rate (higher electric field) is required to obtain penetration. This would suggest that the penetration process is not instantaneous. We study the dynamics of the propagation and penetration process in the next section and report electric field measurements enabling us to compare the electron losses with the electron production.

	Ar (500 μm)	Ar (250 μm)	He (500 μm)	He (250 μm)
$\tau_{ion.\ diff}$ (ms)	5.5	1.4	0.6	0.15
$\tau_{amb.\ diff}$(μs)	70	18	8	2

$\tau_{e.diff}$(ns)	75	20	90	25
$\tau_{diss\text{-}recomb}$(μs)	0.01-0.1		1-10	

Table 2: Electron, ion and ambipolar diffusion time constants for He and Ar plasma jet in capillary tubes with inner diameter of 250 and 500 μm. As a comparison, the bulk electron-ion dissociative recombination time constant is also provided.

3.3 Dynamics of plasma penetration and propagation

Figure 7 shows the evolution of the argon plasma as a function of time for the plasma jet interacting with capillary tubes with an internal diameter of 100 μm, 500 μm and 1.5 mm at 4 mm distance from the jet nozzle. As a comparison, the free jet dynamics is also shown. In the free jet case, the plasma length is increasing during the entire plasma on time and reaches a maximum value of 8 mm. A distance of 4 mm is achieved in less than 3 μs and by placing the capillary tube at a distance of 4 mm, we ensure that the plasma plume will be in contact with the interface of the capillary tube for more than 50% of the plasma time.

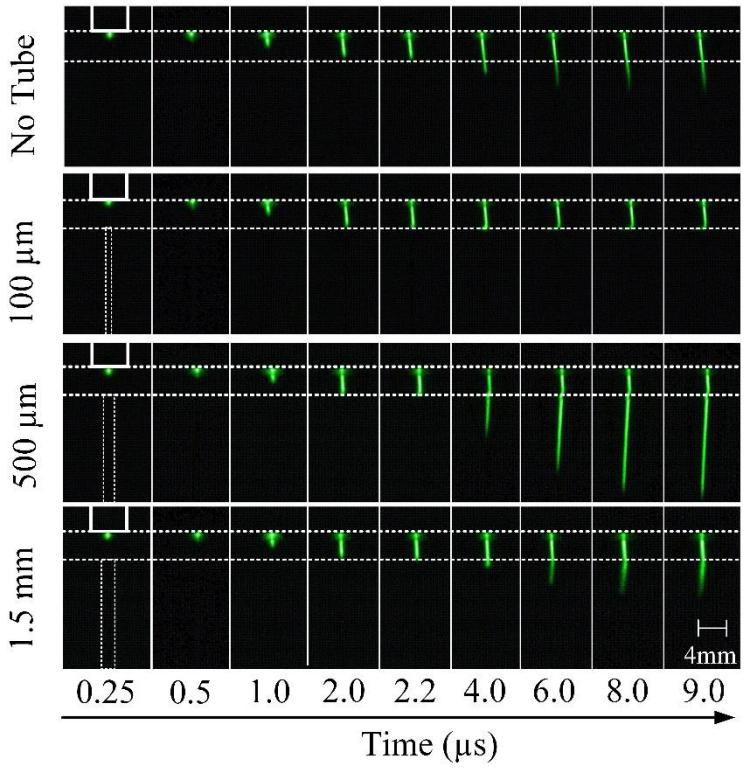

Figure 7: Time resolved images of the argon plasma plume growth including the penetration and propagation process (when occurring) inside capillary tubes with an inner diameter of 100 µm, 500 µm and 1.5 mm at a distance of 4 mm between the nozzle and the capillary tube.

Figure 7 confirms that the plasma jet does not penetrate the 100 µm inner diameter capillary tube. A surface discharge at the position of the capillary tube interface can be clearly observed from 4 µs onward. The argon jet penetrates the 500 µm diameter capillary tube and the plasma length becomes significantly larger than for the free jet. On the other hand, the case of the 1.5 mm diameter tube is more similar to the free jet and this enhancement in plasma plume length is not found. Similar observations have been made for helium. However, in the case of helium the jet penetrates only 1-1.2 mm and a strong ionization wave as in the case of argon was not observed. Therefore, detailed images of the dynamics are not shown for helium.

We will discuss in the next section the penetration process and will come back to the propagation process of the argon jet in the capillary tube the subsequent section.

3.3.1 Penetration

In reported modeling studies related to the penetration of plasma in capillaries the penetration process of the discharge in the capillary is instantaneous [12]. In addition, a helium plasma jet impinging on the outside tube wall of a helium filled tube can lead to the formation of a discharge inside the tube without delay even without direct contact between the discharges outside and inside the tube [18]. However, for the RF discharge we studied, the moment that plasma is in visible contact with the capillary tube does not coincide with the penetration process. Figure 5 shows the times at which the plasma is in contact with the capillary and at which the first penetration of the plasma is observed for different nozzle-capillary distances both for helium and argon impinging on a capillary tube with an inner diameter of 500 μm. The observed delay is between 400-650 ns in argon and 850 and 1500 ns in helium corresponding to several RF cycles. This delay seems occur due to the lower voltages at which RF discharge operate compared to most pulsed discharges that are driven with high over-voltages compared to the breakdown voltage. The delay is not observed for larger tube diameters such as the case of 1.5 mm (Figure 7) and seems to occur when the discharge diameter in the free jet is similar to the capillary tube inner diameter.

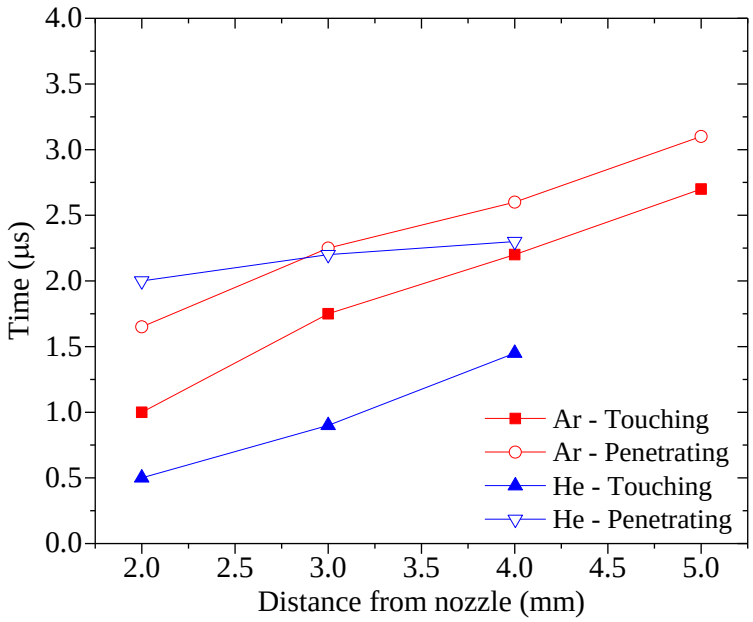

Figure 8: Time at which plasma jet touches and penetrates in a 500 μm capillary tube as a function of distance between the jet nozzle and capillary tube.

This delay is not caused by a significant increase in the electric field between the time of touching and the time of penetration as can be seen from the time resolved electric field waveform in Figure 5. To assess the origin of the delay, it is important to estimate the electric field at the conditions of penetration of the discharge into the capillary tube. Values of the electric field at the interface between plasma and probe are found using the electric field measurement and analysis introduced in the methods section. The values of the measured maximum amplitude of the electric field at the penetration time are used to obtain the electric field inside the crystal.

Figure 9 (a) shows the measured electric field in the crystal as a function of the distance from the jet nozzle to the probe. These measured electric field values in the crystal decrease with increasing distance for the helium jet but remain constant for argon within the experimental accuracy with the exception of the higher measured electric field at 2 mm. The corresponding calculated electric field values at the plasma-probe interface are shown in figure 9 (b). The uncertainty on the surface

electric field measurement is larger than the uncertainty of the measured electric field in the crystal due to the uncertainty in the surface area of the surface charge deposited by the discharge on the probe. The local reduced electric field will be at most 20 Td for Ar and He. We will focus the following discussion on the argon case, but similar conclusion can be drawn for He.

At a reduced electric field of 20 Td, the ionization frequency (due to electron induced ionization of ground state Ar) as calculated by Bolsig [26] with the cross sections taken from [27] equals 7×10^5/s. This ionization frequency is one to two orders of magnitude lower than the electron-ion dissociative recombination frequency for which the time constants are shown in Table 2. Hence, the penetration process at these low voltages requires another ionization source. In an AC driven discharge, it typically takes several discharge cycles to build up the metastable and charged species densities [17, 28]. This has also been observed in a similar RF jet in [17]. Full collisional radiative models can be used to calculate the ionization frequency to consider also stepwise ionization from metastable and excited states and Penning ionization [29]. This approach yields an ionization frequency in Ar at a typical electron energy of 1.5 eV equal to 7.6×10^7, similar to the estimated electron-ion dissociative recombination rate and electron diffusion losses in the 500 μm capillary. Hence, the buildup of metastable and charged species is required to enable sufficient ionization to compensate for the enhanced electron losses during the penetration process.

The same mechanism is responsible for the delay of penetration observed in helium although in view of the larger uncertainty in the surface electric field values and the

strong dependence of the ionization frequency on the unknown air concentration, a quantitative analysis is not possible without detailed knowledge of the air concentration.

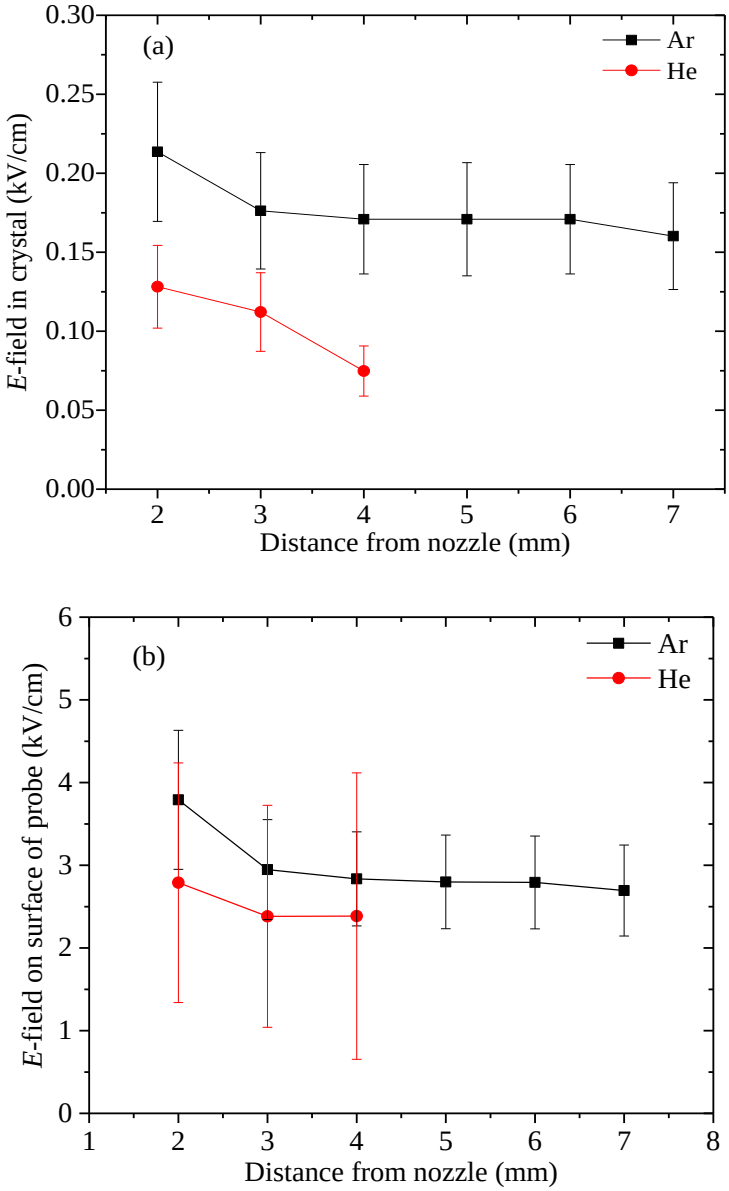

Figure 9: (a) Electrical field inside the crystal as measured as a function of distance between the jet nozzle and probe surface for both helium and argon plasma jet. (b) Electrical field at the surface of the probe as a function of distance between the jet nozzle and probe surface for both helium and argon plasma jet.

3.3.2 Propagation

Most of the studies related to propagation of discharges in capillary tubes deal with ionization fronts generated by pulsed or AC discharges [14,24,31]. The dynamics

of an identical RF plasma has been studied previously in open air [19,30] and we extend this here to include the dynamics of the penetration and propagation process in a capillary tube. The plasma plume length in both argon and helium is plotted for various tube diameters in figure 7 and 8. The corresponding propagation velocities for both helium and argon are in the range of 10^3 to 10^4 ms^{-1}. In pulsed or lower frequency AC discharges, the propagation velocity in helium is often of the order of 10^5-10^8 ms^{-1} [14]. These large differences are however not inconsistent. The temporal and spatial resolved emission of short-lived N_2 (C) and long-lived NO(A) state have been measured in an identical RF driven plasma jet allowing to obtain information about the growth of the ionization wave during one RF cycle and the global growth of the plasma channel length (as provided in figure 7) during the entire modulation cycle [19]. The phase resolved measurements were made possible through the addition of air which reduced the effective lifetime of N_2(C) well below half a period of the discharge cycle. The results showed velocities of ionization fronts up to 7×10^5 ms^{-1} however the average growth of the plume length reduced by two order of magnitude down to 7×10^3 ms^{-1} at distances of a few mm from the nozzle. Hence, the ionization front velocity during one RF cycle is in the same range as the reported values for pulsed and low frequency AC driven discharges but the increase in plume length over several RF cycles occurs at a much smaller velocity.

In the case of argon, for a capillary tube with an inner diameter of 500 μm, the rapid increase in the plume length after penetration inside the capillary tube suggests that the propagation velocity increases. This is however not observed for the capillary tube diameter of 1.5 mm or for helium (see figure 11). The effect of tube diameter on the propagation speed has been studied in detail by Jansky *et al* although in air [33]. They found an increasing velocity with decreasing tube length from 300 to 100 μm.

The propagation velocity reduces however for smaller and higher tube diameters. This effect was correlated with a transition from a surface discharge to a homogeneous streamer discharge filling the entire tube. Xiong *et al* showed that streamers propagating in a dielectric tube can be enhanced due to charging of the tube wall [31].

In the case of negative streamers, if charging occurs in front of the streamer heat, it can align the electric field parallel with the axis of symmetry of the tube and enforce streamer propagation [31]. However, the jet propagation occurs in the positive discharge cycle, and this effect cannot explain the observed phenomenon.

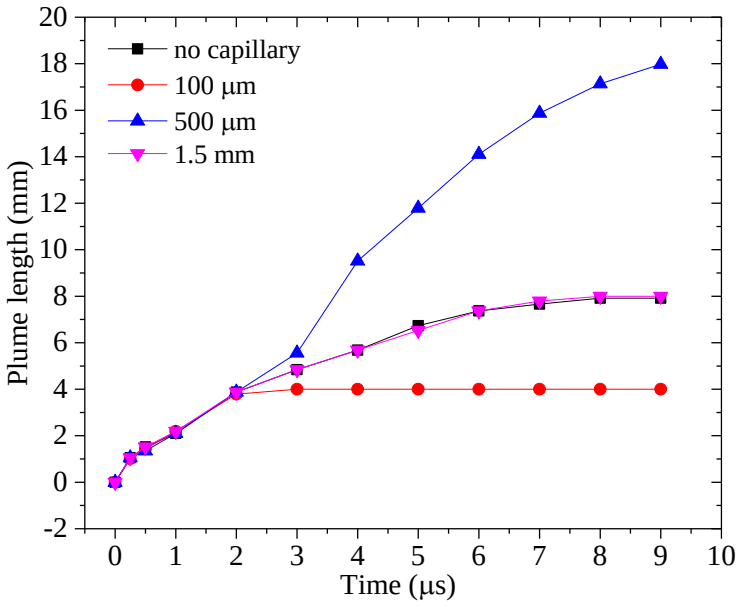

Figure 10: Plume length as a function of time during one modulation cycle for the argon plasma jet impinging onto capillary tubes with inside diameter of 100 µm, 500 µm and 1.5mm at 4mm distance from the jet nozzle.

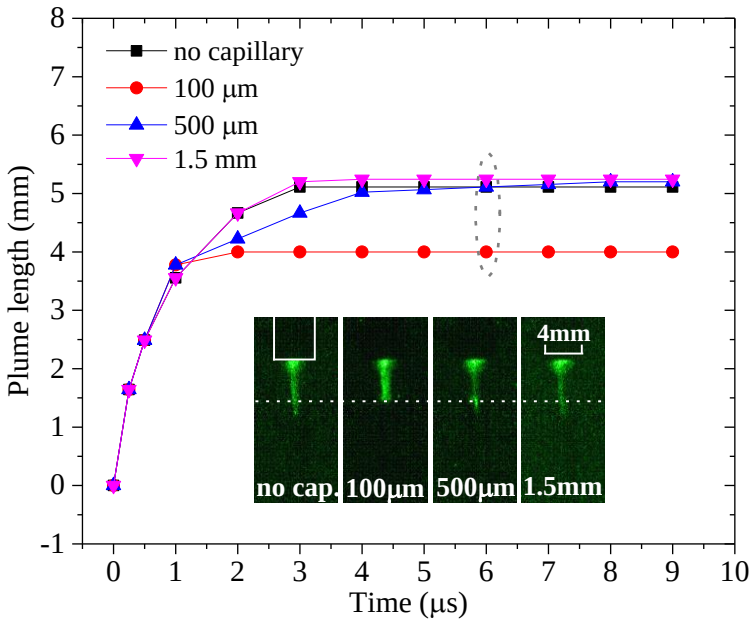

Figure 11: Plume length as a function of time during one modulation cycle for the helium plasma jet impinging onto capillary tubes with inside diameter of 100 µm, 500 µm and 1.5mm at 4mm distance from the jet nozzle. The insert shows ICCD images recorded at 6 µs.

Interestingly, strong emission of $N_2(C)$ produced by electron excitation was only observed once during the period of the excitation frequency for the same jet in Ar + 1% air suggesting that the discharge is only intense for the positive polarity of the excitation cycle [19]. Much stronger emission and propagation during the positive compared to the negative discharge cycle has also been found for the kINPen in a more detailed phase resolved study [30].

Figure 12 shows images taking with an integration time of a quarter of a period. While emission is observed for every image, the strongest emission is always observed for the positive rising voltage that includes the voltage maximum. This was observed in every cycle during the propagation in air and after penetration in the capillary tube. The smaller change in intensity compared to [19] is due to the lack of air in the argon (or helium) feed gas which significantly increased the effective lifetime of the excited states responsible for the observed emission.

The propagation of the jet occurs after this intense re-ignition both in the gas phase and the capillary tube. This is consistent with the idea suggested by Schmidt-Bleker *et al* [30] that in the gas phase, electron loss leads to the formation of negative ions by attachment to O_2 in the surrounding air. The resulting electric field can contribute to the focusing of the electrons to the discharge axis of the jet and also prevents ionization waves from propagating in radial direction [30]. The propagation of the ionization wave is more efficient for argon in the 500 μm tube because this focusing mechanisms is more efficient in the tube compared to free air surrounding as negative ions might diffuse outward (reducing the space charge density) while the surface charge is contained by the dielectric capillary tube interface. The resulting radial electric filed at the edge of the discharge filament focuses the electrons to the capillary tube axis and enhances streamer propagation. This enhancement is not observed in helium because the electron diffusion towards the wall in helium dominate the total electron loss and seems not to be able to be balanced with an increased ionization rate. Hence, the plume length of helium in the capillary tube is not larger than the case of the free jet as can be seen in Figure 11.

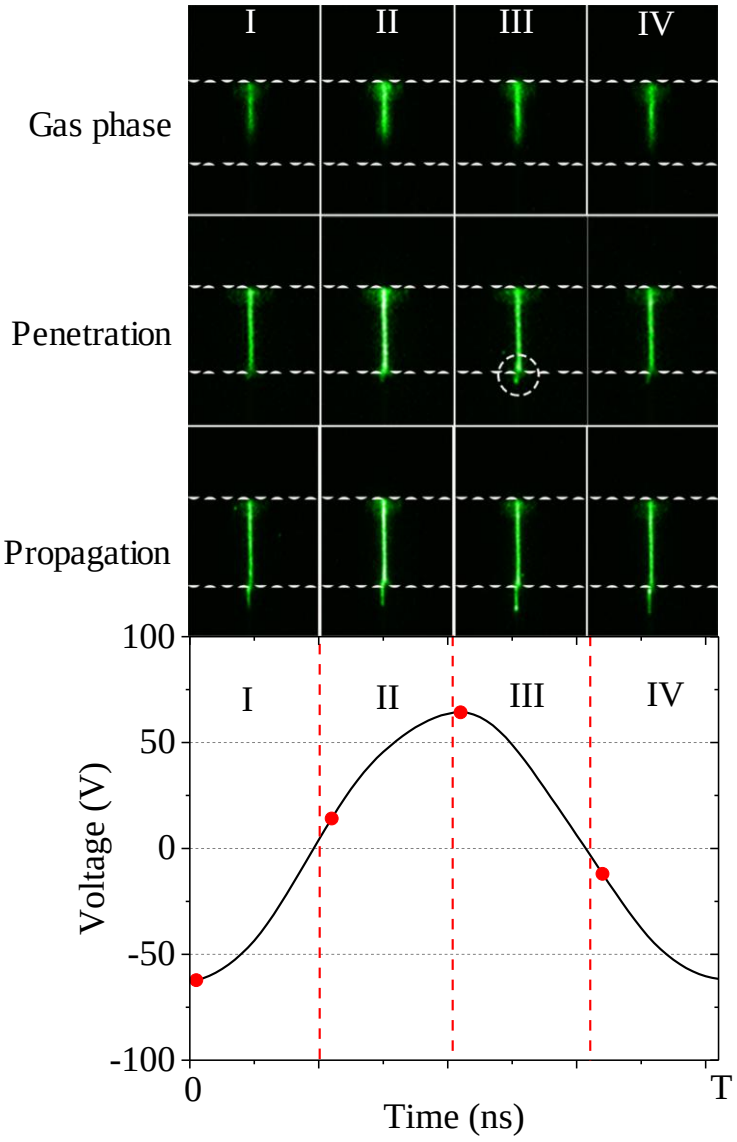

Figure 12: ICCD images with exposure time of ¼ period for argon plasma jet impinging onto a capillary tube with an internal diameter of 500 µm with a distance of 4 mm between jet nozzle and capillary tube surface.

4. Conclusion

The objective of this work was to experimentally investigate the plasma penetration and propagation mechanism inside capillary tubes of varying cross section for RF sustained helium and argon plasmas, operating at low voltages.

It was found that both helium and argon plasma jets do not penetrate into capillary tubes with an inner diameter of 250 μm or smaller. However, the presence of a grounded metal ring electrode enabled the argon plasma jet was able to penetrate inside the 250 μm capillary tube. The plasma plume diameter in the free jet, 350 ± 80 μm and 675 ± 80 μm for the argon and helium jet respectively, is significantly larger than the lowest tube size in which penetration is observed.

The plasma dynamics in capillary tube with an inner diameter of 1.5 mm is very similar to the free jet, however when the tube diameter is similar to the plasma diameter difference can be observed. In the case of helium, the propagation of the discharge into the 500 μm capillary tube is limited to 1-2 mm whereas in argon in the same capillary tube the propagation can be as long as 2 cm for the investigated conditions.

The discharge propagation occurs in the positive discharge cycle both in the free jet and in the capillary. The charging of the capillary tube by electrons will create a radial electric field that focuses electrons onto the capillary tube axis and can enhance streamer propagation. Such enhancement is not observed in helium, most likely because the Debye length is similar as the tube diameter and the formation of a sheath at the plasma-tube interface significantly reduces the bulk plasma volume which drastically enhances the diffusion losses.

The delay between touching and penetration was found to be 400-650 ns for argon and 800-1000 ns for helium. This delay is the result of the small local reduced

electric field which is at most 20 Td for Ar and He. At these low electric fields, Penning and stepwise ionization are required to sustain the plasma and enable penetration. Hence, the requirement to build up these charged and metastable species, which typically takes several RF cycles, can explain the observed delay between touching and penetration.

Bibliography

1. Chu P. K., Lu X., Low Temperature Plasma Technology – Methods and Applications, CRC Press - Taylor & Francis Group, Boca Raton, FL, USA, (2013).
2. Heinlin J., Morfill G., Landthaler M., Stolz W., Isbary G., Zimmermann J. L., Shimizu T., Karrer S., Plasma medicine: possible applications in dermatology, JDDG: Journal der Deutschen Dermatologischen Gesellschaft, 8: 968-976, (2010).
3. Fridman G., Friedman G., Gutsol A., Shekhter A. B., Vasilets V. N., Fridman A., Applied Plasma Medicine, Plasma Process. Polym., 5, 503–533, (2008).
4. Hammer T., Application of Plasma Technology in Environmental Techniques, Contrib. Plasma Phys., 39-5, 441-462, (1999).
5. Bourke P., ziuzina D., Han L., Cullen P. J., Gilmore B. F., Microbiological Interaction with Cold Plasma, Journal of Applied Microbiology, 123, 308—324, (2017).
6. Szili E. J., Hong, S. H., Oh, J.-S., Gaur, N, Short, R.D., Tracking the Penetration of Plasma Reactive Species in Tissue Models, Trends in Biotechnology, 10, 1016, (2017).
7. Foest R., Kindel E., Ohl A., Stieber M. and Weltmann K-D, Non-thermal atmospheric pressure discharges for surface modification, Plasma Phys. Control. Fusion 47, 12B, (2005).
8. Zhang Y., Laer K V, Neyts E. C., Bogaerts A., Can Plasma Be Formed in Catalyst Pores? A Modeling Investigation, Applied Catalysis B: Environmental 185, 56-67, (2016).

9. Zhang Y., Neyts E. C., Bogaerts A., Influence of Material Dielectric Constant on Plasma Generation inside Catalyst Pores, J. Phys. Chem C 120, 25923-25934, (2016).

10. Kunhardt E. E., Generation of Large Volume, Atmospheric-Pressure, Nonequlibrium Plasmas, IEEE Trans. Plasma Sci., 28-1, 268-270, (2000).

11. Hensel K., Martisovits V, Machala Z., Janda M, Lestinsky M, Tardiveau P., Mizuno A., Electrical and Optical Properties of AC Microdischarges in Porous Ceramics, Plasma Process. Polym. 4,682-693, (2007).

12. Zhang Y, Wang H-Y, Zhang Y-R and Bogaerts A, Formation of microdischarges inside a mesoporous catalyst in dielectric barrier discharge plasmas, Plasma Sources Sci. Technol. 26, 054002, (2017).

13. van Gils C.A.J., Hofmann S., Boekema B.K.H.L., Brandenburg R. and Bruggeman P. J., Mechanisms of bacterial inactivation in the liquid phase induced by a remote RF cold atmospheric pressure plasma jet, J. Phys. D: Appl. Phys. 46, 175203, (2013).

14. Jánský J., Algwari Q. T., O'Connell D., and Bourdon A., Experimental–Modeling Study of an Atmospheric-Pressure Helium Discharge Propagating in a Thin Dielectric Tube, IEEE Trans. Plasma Sci., 40-11, 2912-2919 (2012).

15. Naidis G. V., Modelling of plasma bullet propagation along a helium jet in ambient air, J. Phys. D: Appl. Phys. 44, 215203, (2011).

16. Xiong Z., Kushner M. J., Atmospheric pressure ionization waves propagating through a flexible high aspect ratio capillary channel and impinging upon a target, Plasma Sources Sci. Technol. 21, 034001, (2012).

17. van Gessel B., Brandenburg R. and Bruggeman P., Electron properties and air mixing in radio frequency driven argon plasma jets at atmospheric pressure,

Appl. Phys. Lett. 103(6) 064103, (2013).

18. Kondeti S., Gangal U., Yatom S., and Bruggeman P., Ag^+ reduction and silver nanoparticle synthesis at the plasma–liquid interface by an RF driven atmospheric pressure plasma jet: Mechanisms and the effect of surfactant J. Vac. Sci. Technol. A 35-6, (2017).

19. van Gessel A.F.H., Alards K.M.J. and Bruggeman P. J., NO production of an atmospheric pressure RF plasma jet, J. Phys. D: Appl. Phys. 46(26), 265202, (2013).

20. Hofmann S., van Gessel A.F.M., Verreycken T. and Bruggeman P., Power Dissipation, Gas Temperature and Electron Density of a Cold Atmospheric Pressure Helium and Argon RF Plasma Jet, Plasma Sources Sci. Technol., 20, 065010, (2011).

21. B.T.J. van Ham, S. Hofmann, R. Brandenburg and P.J. Bruggeman, In situ absolute air, O_3, and NO densities in the effluent of a cold RF argon atmospheric pressure plasma jet obtained by molecular beam mass spectrometry, J. Phys. D: Appl. Phys. 47 224013, (2014).

22. Ellis H. W., Pai R. Y., McDaniel E. W., Mason E. A., and Viehland L. A., Atomic Data and Nuclear Data Tables17, 177–210 (1976).

23. Jõgi I., Talviste R., Raud J., Piip K. and Paris P., The influence of the tube diameter on the properties of an atmospheric pressure He micro-plasma jet J. Phys. D: Appl. Phys. 47, 415202, (2014).

24. Mussard M D V S, Guaitella O., Rousseau A., Propagation of plasma bullets in helium within a dielectric capillary – influence of the interaction with surfaces, J. Phys. D: Appl. Phys 46, 302001, (2013).

25. Wild R., Benduhn J. and Stollenwerk L., Surface charge transport and decay in dielectric barrier discharges, J. Phys. D: Appl. Phys. 47, 435204, (2014).

26. Hagelaar G.J.M. and Pitchford L. C.**,** Solving the Boltzmann equation to obtain electron transport coefficients and rate coefficients for fluid models, Plasma Sci Sources and Tech 14, 722, (2005).

27. Siglo database, private communication, www.lxcat.net, retrieved on April 16, 2018.

28. Sobota A., Dijk J V and Haverlag M., Ac breakdown in near-atmospheric pressure noble gases: II. Simulations, J. Phys. D: Appl. Phys. 44, 224003, (2011).

29. Jonkers J., Sande M., Sola A., Gamero A. and Mullen J V D, On the differences between ionizing helium and argon plasmas at atmospheric pressure, Plasma Sources Sci. Technol. 12, 30, (2003).

30. Schmidt-Bleker A, Norberg S. A., Winter J., Johnsen E., Reuter S., Weltmann K-D and Kushner M. J., Propagation mechanisms of guided streamers in plasma jets: the influence of electronegativity of the surrounding gas, Plasma Sources Sci. Technol. 24, 3, (2015).

31. Xiong Z., Robert E., Sarron V., Pouvesle J-M and Kushner M. J., Atmospheric-pressure plasma transfer across dielectric channels and tubes, J. Phys. D: Appl. Phys. 46, 155203, (2013).

32. Raizer Y, Gas Discharge Physics, Springer-Verlag Berlin Heidelberg, 1991. - ISBN 978-3-642-64760-4.

33. Jansky J., Delliou P-L, Tholin F., Tardiveau P., Bourdon A., Experimental and numerical study of the propagation of a discharge in a capillary tube in air at atmospheric pressure. J Phys. D: Applied Physics, 44 (33), 335201, (2011).

34. Engineering ToolBox (www.EngineeringToolBox.com)